J. Fluid Mech. (2012), *vol.* 691, *pp.* 26–51.
doi:10.1017/jfm.2011.439

Premixed flame propagation in a confining vessel with weak pressure rise

Andrew P. Kelley[1], John K. Bechtold[2]† and Chung K. Law[1]

[1] Department of Mechanical and Aerospace Engineering, Princeton University, Princeton, NJ 08544, USA

[2] Department of Mathematical Sciences, New Jersey Institute of Technology, Newark, NJ 07102, USA

(Received 31 January 2011; revised 24 September 2011; accepted 29 September 2011; first published online 2 December 2011)

The propagation of a premixed flame inside of a confining vessel filled with combustible fluid is determined using large-activation-energy asymptotics. The flame structure is analysed assuming that spatial and temporal variations in the transverse direction are weak compared to those in the direction normal to the flame surface. The analysis considers weak pressure rise from confinement and also allows for mixtures that are both near and removed from stoichiometry, non-unity reaction orders, temperature-dependent transport coefficients, and general Lewis numbers. The resulting equations for flame propagation speed are expressed in a coordinate-free form and describe the evolution of an arbitrary shaped flame in a general confining flow. These expressions are specifically applied to the case of a spherical flame propagating inside a spherical chamber. The radius at which the confining vessel influences the flame propagation is determined and the various mechanisms influencing flame behaviour are discussed. The results give rise to a simplified asymptotic relationship that provides an improved equation that may be used to more accurately extrapolate unstretched laminar flame speeds from experimental measurements.

Key words: combustion, flames

1. Introduction

In many practical and experimental configurations, premixed flame propagation takes place inside a constant-volume vessel. As a flame propagates through the unburned gas, the pressure inside the vessel begins to rise. This increase in pressure induces a flow field and additionally heats the gases through adiabatic compression. The flame is affected in two ways: the pressure-induced flow field advects the flame surface while the compression and concomitant heating of the gas modifies the chemical reaction rate and thus the flame propagation rate.

Mathematical descriptions of the propagation of confined premixed flames have generally treated the flame as an infinitesimally thin surface of density discontinuity separating the unburned and burned gases. The subsequent analysis of the bulk flow determines the pressure inside the vessel as a function of the location of the flame sheet. In order to complete the formulation, the location of the flame sheet must be determined. One approach is to simply prescribe the flame speed while more formal

† Email address for correspondence: john.k.bechtold@njit.edu

theories analyse the details of the flame structure to derive an explicit expression for the evolution of the flame front.

The earliest theoretical treatments of confined flames (e.g. Eschenback & Agnew 1958; Lewis & von Elbe 1961; Raezer 1961) were primarily concerned with deriving relations between burning velocity and pressure to be used in determining, from experimental data, burning velocities of flames in closed spherical chambers. Bradley & Mitcheson (1976) proposed several phenomenological relations between flame speed and temperature and pressure in their comparison of theory and computations using the same spherical geometry. Sivashinsky (1979) extended these works by adopting an explicit expression for flame speed, previously derived by Bush & Fendell (1970) for unconfined flames, that exhibits a dependence on both pressure and temperature. Chen, Burke & Ju (2009) analysed confined flame propagation by prescribing a flame speed which depends linearly on curvature but did not account for the modification of the reaction rate by compression as was done by Sivashinsky (1979).

The structure of flames propagating with pressure variations either imposed or as a result of confinement have been rigorously analysed previously. In order to constrain the reaction rate term, two methods have primarily been employed in the analysis to restrict the flame temperature to being adiabatic to leading order. The first method restricts the analysis to flames with large exothermicity (e.g. Peters & Ludford 1983; Keller & Peters 1994) while another method restricts the pressure variations to being small (Buckmaster & Lee 1992). These previous derivations were performed for specific flame geometries of planar flames (Peters & Ludford 1983) and spherical flames (Buckmaster & Lee 1992) for general Lewis numbers, while Keller & Peters (1994) analysed general shaped flames with Lewis numbers bounded near unity. Later, Bechtold & Matalon (2000) adopted a delta function model of the reaction zone to allow for larger pressure variations in deriving a Markstein number.

The present work generalizes many of the above studies by considering arbitrary shaped confined flames with non-unity Lewis number, while additionally allowing for near-stoichiometric mixtures, arbitrary reaction orders, and temperature-dependent transport coefficients. The analysis is restricted to a small pressure rise such that the leading-order flame temperature is unperturbed from its adiabatic value. Nevertheless, the present analysis captures the effect of the onset of pressure variations on flame propagation, which is often the critical parameter of interest in experiments. Such is the case with nearly constant-pressure combustion bombs used in the measurement of laminar flame speeds. Therefore, the present analysis is of significant importance in determining conditions under which pressure effects become significant.

The present work provides additional analytical results which are particularly useful for experimentalists using combustion bombs to measure laminar flame speeds. As laminar flame speeds are often used in chemical kinetic mechanism validation, increasingly sophisticated measurement techniques are required to reduce the systematic errors associated with these measurements. One of the largest errors associated with this measurement technique is in the extrapolation of the experimental data to remove the influence of flame stretch. While the present derivation will provide a limit for the largest radius of such a flame where the isobaric assumption is still valid, the data at smaller radii are necessarily stretched. Therefore, the present work extends upon our previous publication (Kelley & Law 2009) by providing an improved equation relating stretch and flame speed which may be used for extrapolating experimental data. As was seen in Kelley & Law (2009), the assumption that the Lewis number is approximately unity is often mathematically advantageous, but is often not the case experimentally. Therefore, the present derivation will allow general

Lewis numbers in order to capture the nonlinear trend in the relationship between stretch and flame speed.

In § 2, the mathematical model and approximations are presented. Asymptotic methods are used to analyse the flame structure, resulting in explicit expressions for the flame propagation rate and its dependence on stretch, flame acceleration, and confinement. The approach is to exploit the disparity in length scales associated with the flame structure and the bulk flow. On the length scale associated with flame thickness, the problem is independent of the confining volume geometry and the local structure analysis is therefore applicable to all confined premixed flames in large vessels. When viewed on the larger hydrodynamic length scale, the flame appears as a surface of density discontinuity advected and distorted by the flow. The present formulation is general and in § 3 the specific case of a spherical flame propagating in a spherical chamber is presented to both elucidate the methodology of analysing the larger length scale and to provide physical insight into the factors which primarily influence the flame propagation. This analysis is extended in § 4 to determine an accurate method of extrapolating unstretched laminar flame speeds from experimental data.

2. Mathematical analysis of the generalized flame

2.1. *Model*

Consider a flame of arbitrary shape propagating through a confining chamber and experiencing a rise in pressure. Assuming that the complex chemistry associated with premixed flame propagation may be described by a one-step, irreversible, overall reaction between two reactants, $\mathscr{M}_E$ the excess reactant and $\mathscr{M}_D$ the deficient reactant, which react to form a product $\mathscr{M}_P$, the reaction is given by

$$\nu_E \mathscr{M}_E + \nu_D \mathscr{M}_D \rightarrow \nu_P \mathscr{M}_P,$$

where ν represents the number of moles of each species.

To obtain physically meaningful quantities, all variables are non-dimensionalized. The thermodynamic variables, species concentrations, and transport properties are non-dimensionalized with respect to their values in the initial, unburned state. The laminar flame speed, $\tilde{s}_u^0$, defined as the speed with which a planar flame propagates into the unburned gas, is used as a characteristic speed. A characteristic length scale, $\tilde{L}$, is adopted, which is a measure of the vessel size or the bulk flow, and a characteristic time scale is thus $\tilde{L}/\tilde{s}_u^0$. Dimensional quantities are denoted with a tilde, initial conditions with the superscript 0, unburned gas conditions with subscript u, and burned gas conditions with subscript b.

Several standard assumptions are made in the present analysis. The flame is assumed to propagate slowly relative to the speed of sound (small Mach number, M_u^0) such that, to leading order, the pressure is spatially uniform but varies with time and may be expressed as $P(t) + \gamma\,(M_u^0)^2\,p(\boldsymbol{x}, t)$ where γ is the ratio of specific heats. Higher-order diffusivity is assumed negligible and therefore only Fickian mass diffusion is considered. Diffusivity of each species, i, is defined by a characteristic diffusivity relative to the mixture, $\tilde{D}_i$. The thermal diffusivity $\tilde{\lambda}$, mass diffusivity $\tilde{D}_i$, and viscosity $\tilde{\mu}$, are assumed to vary with temperature but the Lewis number Le_i and Prandtl number Pr, are assumed to remain constant.

Under these assumptions, the governing equations in non-dimensional form may now be written (e.g. Williams 1994)

Continuity:

$$\frac{\mathrm{D}\rho}{\mathrm{D}t} + \rho(\boldsymbol{\nabla}\cdot\boldsymbol{V}) = 0, \tag{2.1}$$

Species:

$$\rho\frac{\mathrm{D}Y_i}{\mathrm{D}t} - \frac{\delta}{Le_i}\boldsymbol{\nabla}\cdot(\lambda\boldsymbol{\nabla}Y_i) = -\frac{\omega}{(1+\epsilon\varphi_i)\epsilon}, \tag{2.2}$$

Momentum:

$$\rho\frac{\mathrm{D}\boldsymbol{V}}{\mathrm{D}t} = -\boldsymbol{\nabla}p + \delta Pr\boldsymbol{\nabla}\cdot\left[\lambda\left\{\boldsymbol{\nabla}\boldsymbol{V} + (\boldsymbol{\nabla}\boldsymbol{V})^{\mathrm{T}} - \tfrac{2}{3}\mathscr{I}(\boldsymbol{\nabla}\cdot\boldsymbol{V})\right\}\right]. \tag{2.3}$$

Energy:

$$\rho\frac{\mathrm{D}T}{\mathrm{D}t} - \delta\boldsymbol{\nabla}\cdot(\lambda\boldsymbol{\nabla}T) = \frac{\gamma-1}{\gamma}\frac{\mathrm{d}P}{\mathrm{d}t} + q\frac{\omega}{\epsilon} \tag{2.4}$$

where i represents either the excess (E) or deficient (D) reactant, $\mathrm{D}/\mathrm{D}t$ is the Lagrangian derivative, $\mathscr{I}$ the unit tensor, the reaction rate is

$$\omega = Da_C T^{\alpha} Y_D^a Y_E^b \rho^{a+b} \exp\left(-\frac{E_a}{T}\right) \tag{2.5}$$

and the gas is assumed to be ideal,

$$P = \rho T. \tag{2.6}$$

The symbols used above represent the variables density ρ, temperature T, species mass fraction Y, velocity vector $\boldsymbol{V}$, heat release q, collisional Damköhler number Da_C, reaction order of deficient species a, reaction order of excess species b, pre-exponential temperature dependence α, activation energy E_a, and the relative flame thickness δ to be defined later. An inverse Zeldovich number has been defined as $\epsilon = T_{ad}^2/E_a$, where T_{ad} is the adiabatic flame temperature. The largeness of the activation energy will be exploited and thus it is assumed that ϵ is a small parameter.

The mixture strength is defined by $\phi = \tilde{Y}_E^0\nu_D\tilde{W}_D/\tilde{Y}_D^0\nu_E\tilde{W}_E$, where $\tilde{W}$ is the molecular weight. As defined, ϕ is identical to the equivalence ratio for mixtures in which the fuel is the excess reactant, and is the reciprocal of the equivalence ratio when the fuel is deficient. From this definition, it follows that ϕ is always greater than unity. Further, it is assumed that conditions are very close to stoichiometry, $\phi = 1 + \epsilon\varphi$, where φ is order one, and consequently both reactants are consumed to leading order. Note that results corresponding to off-stoichiometric mixtures are recovered in the limit $\varphi \to \infty$. To simplify the writing of the species equations, φ_i is defined such that $\varphi_E = \varphi$ and $\varphi_D = 0$.

The above equations may be analysed by exploiting the differences in length scales present in the problem. The hydrodynamic length scale, $\tilde{L}$, is the largest scale and describes the bulk fluid motion. When viewed on this scale, diffusion and chemical reaction are confined to a thin sheet which separates burned from unburned gases. The small scale, on which diffusion occurs, is the laminar flame thickness, $\tilde{\ell} = \tilde{\lambda}^0/\tilde{c}_p\tilde{\rho}^0\tilde{s}_u^0$, where $\tilde{c}_p$ is the specific heat at constant pressure. The ratio of these two length scales, $\delta = \tilde{\ell}/\tilde{L}$, is a small parameter that may be exploited in an asymptotic strategy.

Furthermore, for the realistic case of large activation energy, the chemical reaction zone is confined to a yet thinner region of order $\epsilon\delta$ within this zone. A similar model was employed by Matalon, Cui & Bechtold (2003) and was analysed for the case of constant pressure and near unity Lewis number.

The present analysis describes slow variations, and thus the distinguished limit, $\epsilon = \delta$, is considered. This assumes that the reaction zone is an order of magnitude smaller than the diffusion zone and uniquely defines the characteristic length scale used in the non-dimensionalization of the governing equations such that $\tilde{L} = \tilde{\ell} E_a / T_{ad}^2$.

The magnitude of the pressure rise due to confinement may be determined by multiplying the continuity equation by T and adding it to the energy equation,

$$\frac{1}{\gamma}\frac{\mathrm{d}P}{\mathrm{d}t} + P(\boldsymbol{\nabla}\cdot\boldsymbol{V}) = \epsilon\boldsymbol{\nabla}\cdot(\lambda\boldsymbol{\nabla}T) + q\frac{\omega}{\epsilon}. \tag{2.7}$$

This may be integrated, along with the species equation, over the volume of the vessel, $\mathscr{V}$, to determine the pressure inside the vessel (e.g. Bechtold & Matalon 2000),

$$P = 1 + q\gamma\left(1 - \frac{m_D}{\mathscr{V}}\right), \tag{2.8}$$

where the walls of the vessel are assumed adiabatic. The total mass of the deficient reactant in the vessel as a function of time, m_D, is equal to the integral of ρY_D over the volume of the vessel. The initial value of m_D is $\mathscr{V}$ and m_D vanishes after the entire vessel has been combusted. It may be seen that, as long as m_D is relatively close to the initial value of $\mathscr{V}$, the pressure will not change appreciably. This is the case when the volume of the flame is small relative to the volume of the confining vessel, and thus the present investigation will be restricted to flames with an average radius less than about half of the average radius of the confining volume. It is thus appropriate to introduce the expansion $P(t) = 1 + \epsilon\hat{P}(t)$, and consider the effect of the weak pressure perturbation on the dynamics of the flame front. Ahead of the flame front, the unburned gas is adiabatically compressed. In the limit of weak pressure rise, the unburned gas temperature is $T_u = 1 + \epsilon\hat{P}(1 - 1/\gamma) + O(\epsilon^2)$.

2.2. *Analysis of the flame structure*

The bulk flow for a particular configuration is described by the above equations with reaction and diffusion ignored. However, in order to relate the flow variables on either side of the flame surface, it is necessary to analyse the details of the structure. To do so, it is convenient to adopt a coordinate system attached to the flame surface. Let the surface of the flame be defined by the function $F(x, y, z, t) = 0$. A Cartesian coordinate system attached to the flame surface is defined by $\xi \equiv (x - f(y, z, t))/\epsilon$, $\hat{y} \equiv y$, $\hat{z} \equiv z$, and $\hat{t} \equiv t$ where $F(x, y, z, t) = x - f(y, z, t)$. By introducing the dependence of ξ on ϵ^{-1}, the present analysis is in a reference frame where derivatives normal to the flame will be much larger than those in time and the other spatial directions. This corresponds to the slowly varying flame analysis of Buckmaster & Ludford (1982). The velocity vector $\boldsymbol{V}$ will be decomposed as $\boldsymbol{V} \to (u, \boldsymbol{v})$. On the ξ length scale, the reaction is confined to a narrow zone located at $\xi = 0$ which has thickness of order ϵ. In this coordinate system, the following relations may be obtained:

$$\boldsymbol{\nabla} = \left(\frac{\partial}{\partial x}, \frac{\partial}{\partial y}, \frac{\partial}{\partial z}\right) = \frac{\boldsymbol{i} - \boldsymbol{\nabla} f}{\epsilon}\frac{\partial}{\partial \xi} + \hat{\boldsymbol{\nabla}}_s, \tag{2.9}$$

where

$$\hat{\boldsymbol{\nabla}}_s = \left(0, \frac{\partial}{\partial \hat{y}}, \frac{\partial}{\partial \hat{z}}\right) \quad \text{and } \boldsymbol{i} \text{ is the unit vector in the } x\text{-direction.} \tag{2.10}$$

Furthermore, employing a weighted coordinate system simplifies some complications that arise from the variable transport assumption. In order to handle the temperature dependence of the transport parameter, λ, it is convenient to introduce an inverse transport weighted coordinate system, $(\eta, \bar{y}, \bar{z}, \bar{t})$, where

$$\eta = \int_0^{\xi} \frac{1}{\lambda(\theta, \hat{y}, \hat{z}, \hat{t})}\, \mathrm{d}\theta, \tag{2.11}$$

$\bar{y} \equiv \hat{y}$, $\bar{z} \equiv \hat{z}$, and $\bar{t} \equiv \hat{t}$. In this coordinate system, the gradient may be written as

$$\boldsymbol{\nabla} = \frac{\boldsymbol{i} - \boldsymbol{\nabla} f}{\epsilon \lambda} \frac{\partial}{\partial \eta} + \hat{\boldsymbol{\nabla}}_s \eta \frac{\partial}{\partial \eta} + \bar{\boldsymbol{\nabla}}_s, \tag{2.12}$$

where the mass flux is defined as $m \equiv \rho s$, with

$$s = \frac{1}{N}\left(u - \boldsymbol{v} \cdot \boldsymbol{\nabla} f - \frac{\partial f}{\partial t}\right) \tag{2.13}$$

and

$$N = \sqrt{1 + |\boldsymbol{\nabla} f|^2}. \tag{2.14}$$

Note that the gradient and transverse gradient of f are identical in each coordinate system.

In this coordinate system the continuity, species, and energy equations are

$$N \frac{\partial m}{\partial \eta} + \epsilon \lambda \left[\frac{\partial \rho}{\partial \bar{t}} + \bar{\boldsymbol{\nabla}}_s \cdot (\rho \boldsymbol{v}) + \rho \hat{\boldsymbol{\nabla}}_s \eta \cdot \frac{\partial \boldsymbol{v}}{\partial \eta} + \frac{\partial \rho}{\partial \eta}\left(\frac{\partial \eta}{\partial \hat{t}} + \boldsymbol{v} \cdot \hat{\boldsymbol{\nabla}}_s \eta\right)\right] = 0, \tag{2.15}$$

$$Nm \frac{\partial Y_i}{\partial \eta} + \epsilon \lambda \rho \left[\frac{\partial Y_i}{\partial \bar{t}} + \boldsymbol{v} \cdot \bar{\boldsymbol{\nabla}}_s Y_i + \frac{\partial Y_i}{\partial \eta}\left(\frac{\partial \eta}{\partial \hat{t}} + \boldsymbol{v} \cdot \hat{\boldsymbol{\nabla}}_s \eta\right)\right] = \frac{\lambda}{Le_i} \Delta Y_i - \frac{1}{1 + \epsilon \varphi_i} \lambda \omega, \tag{2.16}$$

$$Nm \frac{\partial T}{\partial \eta} + \epsilon \lambda \rho \left[\frac{\partial T}{\partial \bar{t}} + \boldsymbol{v} \cdot \bar{\boldsymbol{\nabla}}_s T + \frac{\partial T}{\partial \eta}\left(\frac{\partial \eta}{\partial \hat{t}} + \boldsymbol{v} \cdot \hat{\boldsymbol{\nabla}}_s \eta\right)\right] = \epsilon^2 \lambda \frac{\gamma - 1}{\gamma} \frac{\mathrm{d}\hat{P}}{\mathrm{d}\bar{t}} + \lambda q \omega + \lambda \Delta T, \tag{2.17}$$

where Δ is defined

$$\begin{aligned} \Delta &= \epsilon^2 \boldsymbol{\nabla} \cdot (\lambda \boldsymbol{\nabla}) \\ &= \frac{N^2}{\lambda} \frac{\partial^2}{\partial \eta^2} - \frac{\epsilon}{\lambda} \frac{\partial \lambda}{\partial \eta} \left[(\boldsymbol{\nabla} f \cdot \bar{\boldsymbol{\nabla}}_s) + (\boldsymbol{\nabla} f \cdot \hat{\boldsymbol{\nabla}}_s \eta) \frac{\partial}{\partial \eta}\right] \\ &\quad - \epsilon \left[\nabla^2 f \frac{\partial}{\partial \eta} + 2 \boldsymbol{\nabla} f \frac{\partial}{\partial \eta}(\bar{\boldsymbol{\nabla}}_s) + 2 (\boldsymbol{\nabla} f \cdot \hat{\boldsymbol{\nabla}}_s \eta) \frac{\partial^2}{\partial \eta^2} + \boldsymbol{\nabla} f \cdot \frac{\partial}{\partial \eta}(\hat{\boldsymbol{\nabla}}_s \eta) \frac{\partial}{\partial \eta}\right] + O(\epsilon^2). \end{aligned} \tag{2.18}$$

Note that, on the η length scale, the temporal variation of the pressure contributing to the energy equation is of order ϵ^2. Therefore, the influence of the pressure perturbation on the flame structure will only be felt through the matching conditions at $\eta \to \pm\infty$ where the hydrodynamic equations provide boundary conditions on the flame structure.

In the large-activation-energy limit, the reaction zone is confined to a yet thinner layer in which a balance between diffusion and reaction is maintained.

Furthermore it is convenient to define an enthalpy function, $H_i = T + (1 + \epsilon\varphi_i)qY_i$, which simplifies the governing equations by removing the reaction rate term,

$$Nm\frac{\partial H_i}{\partial \eta} + \epsilon\lambda\rho\left[\frac{\partial H_i}{\partial \bar{t}} + \boldsymbol{v}\cdot\bar{\boldsymbol{\nabla}}_s H_i + \frac{\partial H_i}{\partial \eta}\left(\frac{\partial \eta}{\partial \hat{t}} + \boldsymbol{v}\cdot\hat{\boldsymbol{\nabla}}_s\eta\right)\right] = \lambda\Delta H_i + \left(\frac{1}{Le_i} - 1\right)\lambda\Delta(H_i - T) + \epsilon^2\lambda\frac{\gamma - 1}{\gamma}\frac{\mathrm{d}\hat{P}}{\mathrm{d}\bar{t}}. \tag{2.19}$$

On the η length scale, the reaction zone is confined to a region of thickness $O(\epsilon)$ located at $\eta = 0$. Therefore, the flame structure may be resolved by solving the chemically free governing equations on either side of the reaction zone. These equations may now be integrated across the flame zone in the limit of large activation energy, as first demonstrated by Sivashinsky (1976) and Buckmaster (1977). Our analysis follows most closely that discussed in Bechtold & Matalon (1999), who extended the above slowly varying flame (SVF) analyses to include stoichiometric effects and variable transport in the form $\lambda = T$.

In the subsequent analysis, the $O(\epsilon)$ enthalpy $H_{i,1}$ will be needed, but the leading-order solution to all other variables will be sufficient. Note that the subscript 1 corresponds to order-ϵ perturbations. Integrating (2.19) from $-\infty$ to 0^+ yields the $O(\epsilon)$ enthalpy perturbation downstream of the reaction zone,

$$H_{i,1}(0^+) = \frac{\gamma - 1}{\gamma}\hat{P} + \varphi_i q + \frac{1}{s_u^2}\left(\frac{1}{s_u}\frac{\hat{\mathrm{D}}s_u}{\hat{\mathrm{D}}\bar{t}} - \kappa\right)I_i, \tag{2.20}$$

where $\hat{\mathrm{D}}/\hat{\mathrm{D}}\bar{t} = \partial/\partial\bar{t} + [\boldsymbol{v}(-\infty) - s_u\boldsymbol{n}]\cdot\bar{\boldsymbol{\nabla}}$, $s(-\infty) = m_0 = s_u$ which is the velocity of the flame with respect to the unburned gas, and $\boldsymbol{n} = (\boldsymbol{i} - \boldsymbol{\nabla}f)/N$ is a unit normal vector. The flame stretch rate, κ, may be defined from e.g.equation (6.7) in Matalon & Matkowsky (1982),

$$\kappa = \frac{1}{N}\bar{\boldsymbol{\nabla}}_s\cdot[s(-\infty)\nabla f] + \bar{\boldsymbol{\nabla}}_s\cdot\boldsymbol{v}(-\infty) + \frac{1}{N}\frac{\partial N}{\partial t} + \frac{1}{N}\boldsymbol{v}(-\infty)\cdot\bar{\boldsymbol{\nabla}}_s N. \tag{2.21}$$

The integral I_i is defined as

$$I_i = I(\lambda, T_{ad}, Le_i) = \int_1^{T_{ad}}\frac{\lambda}{T}\left[1 - \left(\frac{T-1}{T_{ad}-1}\right)^{Le_i - 1}\right]\mathrm{d}T.$$

Note that for $Le_i > 1$, $I_i > 0$ and for $Le_i < 1$, $I_i < 0$. For the case where $\lambda = T$, $I_i = q(1 - Le_i^{-1})$.

Equation (2.20) contains the pressure perturbation term $\hat{P}$. This term appears from the boundary condition where the enthalpy of the gas entering the flame structure is increased due to adiabatic compression of the unburned gas. This is the only mechanism through which the influence of confinement affects the flame structure and mass burning rate. It is worth noting that combustion-emitted acoustic pressure has been shown to affect the flame speed in the same way (Clavin, Pelcé & He 1990; Wu *et al.* 2003).

One of the two reactants must be completely consumed. To determine which reactant is completely consumed, consider the difference in the enthalpies from (2.20),

$$Y_{E,1}(0^+) - Y_{D,1}(0^+) = \varphi + \frac{1}{qs_u^2}\left(\frac{1}{s_u}\frac{\hat{\mathrm{D}}s_u}{\hat{\mathrm{D}}\bar{t}} - \kappa\right)(I_E - I_D). \tag{2.22}$$

It may be seen that if the right-hand side of (2.22) is positive, reactant $\mathscr{M}_D$ is completely consumed. However, if the right-hand side of (2.22) is negative, the deficient reactant $\mathscr{M}_D$ will leak through the reaction zone and reactant $\mathscr{M}_E$ will be completely consumed.

Equation (2.20) provides one relationship between the enthalpy and the flame speed. In order to uniquely determine these quantities and thus close the problem, the thin region in which chemical reactions are confined must be analysed.

In the reaction zone, the influence of confinement is not directly present. A standard analysis of the reactive layer yields (e.g.Buckmaster & Ludford 1982)

$$s_u^2\mathscr{G}\left(a, b; \frac{q\varphi}{Le_E}\right) = \mathrm{e}^{T_1(0^+)}\int_0^\infty \left(\frac{qY_{D,1}}{Le_D} + \theta\right)^a \left(\frac{qY_{E,1}}{Le_E} + \theta\right)^b \mathrm{e}^{-\theta}\,\mathrm{d}\theta, \tag{2.23}$$

where

$$\mathscr{G}(a, b; S) = \int_0^\infty x^a\,(x + S)^b\,\mathrm{e}^{-x}\,\mathrm{d}x. \tag{2.24}$$

2.3. *Flame evolution equation*

Having solved the flame structure and reaction zones, it is now possible to determine the flame speed as a function of the stretch, acceleration, and confinement. By combining the results of (2.20) and (2.23) an equation describing the evolution of the flame front may be determined. The evolution equation will be shown for three cases: reactant $\mathscr{M}_D$ completely consumed, reactant $\mathscr{M}_E$ completely consumed, and off-stoichiometric mixtures.

For the case where reactant $\mathscr{M}_D$ is completely consumed, let $Y_{D,1}(0^+) = 0$ in (2.22). Equations (2.20) and (2.22) then determine the temperature and species concentration perturbations,

$$Y_{E,1}(0^+) = \varphi + \frac{1}{qs_u^2}\left(\frac{1}{s_u}\frac{\hat{\mathrm{D}}s_u}{\hat{\mathrm{D}}\bar{t}} - \kappa\right)(I_E - I_D)\,, \tag{2.25}$$

$$T_1(0^+) = \frac{\gamma - 1}{\gamma}\hat{P} + \frac{1}{s_u^2}\left(\frac{1}{s_u}\frac{\hat{\mathrm{D}}s_u}{\hat{\mathrm{D}}\bar{t}} - \kappa\right)I_D. \tag{2.26}$$

The temperature perturbation depends on the pressure perturbation, $\hat{P}$. This arises due to the confined unburned gas being heated by isentropic compression before entering the reaction zone. The heating due to isentropic compression is limited to a small perturbation as a result of the small-pressure-rise assumption. Additionally, the T_1 temperature perturbation is modified by the flame acceleration and hydrodynamic stretch. Both of these terms are multiplied by the integral I_D which quantifies the diffusive strength of the mixture.

For the steady planar flame, $Y_{E,1}(0^+) = \varphi$. However, for a general flame, the locally excess reactant concentration is modified. The modification again depends on the flame acceleration and hydrodynamic stretch. Both of these terms are multiplied by the quantity $I_E - I_D$ which quantifies the preferential diffusion of the two species.

Inserting expressions for $Y_{E,1}(0^+)$ and $T_1(0^+)$ into (2.23) and setting $Y_D(0^+) = 0$ yields

$$s_u^2 \ln s_u^2 - s_u^2 \ln \left[\frac{\mathscr{G}\left(a, b; \dfrac{qY_{E,1}\left(0^+\right)}{Le_E}\right)}{\mathscr{G}\left(a, b; \dfrac{q\varphi}{Le_E}\right)} \right] = s_u^2 \frac{\gamma - 1}{\gamma} \hat{P} + \left(\frac{1}{s_u} \frac{\hat{\mathrm{D}} s_u}{\hat{\mathrm{D}}\bar{t}} - \kappa \right) I_D. \quad (2.27)$$

For the case where reactant $\mathscr{M}_E$ is completely consumed, let $Y_{E,1}(0^+) = 0$ in (2.22). Equations (2.20) and (2.22) then determine the temperature and species concentration perturbations,

$$Y_{D,1}(0^+) = -\varphi - \frac{1}{q s_u^2} \left(\frac{1}{s_u} \frac{\hat{\mathrm{D}} s_u}{\hat{\mathrm{D}}\bar{t}} - \kappa \right) (I_E - I_D), \quad (2.28)$$

$$T_1(0^+) = \frac{\gamma - 1}{\gamma} \hat{P} + \varphi q + \frac{1}{s_u^2} \left(\frac{1}{s_u} \frac{\hat{\mathrm{D}} s_u}{\hat{\mathrm{D}}\bar{t}} - \kappa \right) I_E, \quad (2.29)$$

which when inserted into (2.23) yield

$$s_u^2 \ln s_u^2 - s_u^2 \ln \left[\frac{\mathscr{G}\left(b, a; \dfrac{qY_{D,1}(0^+)}{Le_D}\right)}{\mathscr{G}\left(a, b; \dfrac{q\varphi}{Le_E}\right)} \right] = s_u^2 \frac{\gamma - 1}{\gamma} \hat{P} + s_u^2 \varphi q + \left(\frac{1}{s_u} \frac{\hat{\mathrm{D}} s_u}{\hat{\mathrm{D}}\bar{t}} - \kappa \right) I_E. \quad (2.30)$$

Note that, although the present analysis considers near-stoichiometric flames, the result for off-stoichiometric mixtures is recovered in the limit that $\varphi \to \infty$ in (2.27),

$$s_u^2 \ln s_u^2 = s_u^2 \frac{\gamma - 1}{\gamma} \hat{P} + \left(\frac{1}{s_u} \frac{\hat{\mathrm{D}} s_u}{\hat{\mathrm{D}}\bar{t}} - \kappa \right) I_D. \quad (2.31)$$

Equations (2.27) and (2.30) govern flame propagation for near-stoichiometric mixtures. The determination of which of the two equations is controlling depends on the sign of (2.22). For off-stoichiometric mixtures, the flame speed is governed by (2.31).

For an unconfined flame with unity reaction orders and setting $\lambda = T$, the present analysis recovers the result of Bechtold & Matalon (1999). Furthermore, the present analysis recovers the result of Peters & Ludford (1983) if their result is expanded for small pressure perturbations.

The present analysis was carried out within the slowly varying flame (SVF) framework. It is valid for Lewis numbers bounded away from unity, and considers slow evolution on a long time scale. In the next two sections, we will employ our model to investigate the effects of weak pressure rise on the behaviour of spherically expanding flames. It should be noted that SVF models have been used previously to examine the effects of small perturbations and stability on flame evolution (Buckmaster & Ludford 1982) as well as freely expanding flames (Matalon & Bechtold 1987; Ronney & Sivashinsky 1989). These, and other studies, have demonstrated that the SVF formulation generally gives an accurate description of flame behaviour in mixtures with $Le < 1$. However, for $Le > 1$, the model often admits

non-physical solutions. These arise as a result of oscillations, on a fast time scale, that are known to occur for this range of Lewis number, and that are not accounted for in an SVF formulation (Buckmaster & Ludford 1982; Ronney & Sivashinsky 1989). Nevertheless, in the case of a spherically expanding flame with $Le > 1$, the model admits a separatrix solution that accurately describes the acceleration of the flame to a constant speed, consistent with experimental observations (Matalon & Bechtold 1987; Ronney & Sivashinsky 1989). Thus the SVF formulation may provide physical insight into premixed flame propagation, even for $Le > 1$. The results of our work, reported below, are consistent with the findings of these earlier studies.

Note that the above analysis completely resolves the flame structure, incorporating all effects of diffusion and reaction. The equations are useful for any flame configuration. To determine precisely how a flame will behave in a particular flow field, the hydrodynamic equations must be solved on either side of the flame surface. The above equations may then be used to track the evolution of the front. In the next section, the specific case of a spherical flame is analysed propagating either in an infinitely large domain or inside a spherical chamber.

3. Confined spherical flames

One of the most common experimental configurations in which flames propagate in a confinement involves spherical flames ignited by spark discharge. These experiments are often used in the measurement of high-pressure laminar flame speeds. In the present analysis, a confining vessel of spherical shape is considered as this geometry results in a one-dimensional analysis in the radial direction. It should be noted that the dimensionality of the problem can change due to the formation of instabilities on the flame surface (e.g. Jomaas, Law & Bechtold 2007; Pelce & Clavin 1982) but this instability formation is not considered in the present analysis.

The solution to the hydrodynamic equations is similar to that of Sivashinsky (1979). The flow field on either side of the flame may be determined from the governing equations noting that diffusion and reaction are second-order effects. For spherical flames, the continuity equation may be combined with the energy equation as done in (2.7), such that the radial velocity on either side of the flame surface is governed by

$$\frac{1}{\gamma P}\frac{\mathrm{d}P}{\mathrm{d}t} + \frac{1}{r^2}\frac{\partial}{\partial r}(r^2 u) = 0, \tag{3.1}$$

where u is the radial velocity. For a spherical confinement of radius r_w, and flame radius r_f, the following leading-order velocity field is obtained:

$$u = \begin{cases} -\dfrac{r}{3\gamma P}\dfrac{\mathrm{d}P}{\mathrm{d}t}, & 0 \leqslant r < r_f, \\ \dfrac{r}{3\gamma P}\dfrac{\mathrm{d}P}{\mathrm{d}t}\left(\dfrac{r_w^3}{r^3} - 1\right), & r_f < r \leqslant r_w. \end{cases} \tag{3.2}$$

From the jump relation for the mass flux across the reaction zone, and isentropic compression of the unburned gas, the following relationship is obtained:

$$\frac{1}{\gamma}\frac{\mathrm{d}P}{\mathrm{d}t} r_w^3 = q\frac{\mathrm{d}}{\mathrm{d}t}[P^{1/\gamma}(r_f^3 - r_w^3)], \tag{3.3}$$

which may be integrated to yield

$$\frac{P-1}{P_e-1} = 1 - P^{1/\gamma}\left(1 - \frac{r_f^3}{r_w^3}\right), \tag{3.4}$$

which also follows from (2.7), where $P_e = 1 + q\gamma$ is the final pressure after complete combustion of the gas in the vessel.

In order to keep the hydrodynamic derivation consistent with the analysis of the flame zone, the pressure rise must be restricted to be small such that $P = 1 + \epsilon\hat{P}$. Analysing (3.4), it is seen that r_w^{-3} must be $\sim O(\epsilon)$ for the pressure rise to be small. In order to explicitly denote the order of the wall radius, a normalized wall radius is defined,

$$\epsilon r_w^3 = (\hat{R}_w T_{ad} I_D)^3 (\gamma - 1)\frac{q}{T_{ad}}, \tag{3.5}$$

where $\hat{R}_w^3$ is an order-one quantity. Under these conditions (3.4) yields the definition of the pressure perturbation,

$$\hat{P} = \frac{\gamma}{\gamma - 1}\left(\frac{r_f}{\hat{R}_w T_{ad} I_D}\right)^3. \tag{3.6}$$

For the small-pressure-perturbation case, the leading-order velocity field given by (3.2) can be simplified to

$$u = \begin{cases} 0, & 0 \leqslant r < r_f, \\ \dfrac{r_f^2}{r^2}\dfrac{\mathrm{d}r_f}{\mathrm{d}t}\dfrac{q}{T_{ad}}, & r_f < r. \end{cases} \tag{3.7}$$

This velocity field is equivalent to the case of an unconfined spherical flame. This is an interesting result. In some previous studies (e.g. Chen *et al.* 2009), the primary influence of confinement has been attributed to a change in the flow field. However, for flames which are weakly affected by confinement, the primary influence of confinement is through a modification of the flame speed as a result of the isentropic compression of the unburned gas.

In the subsequent analysis, the definition of a normalized flame radius simplifies the notation,

$$r_f \equiv R_f T_{ad} I_D. \tag{3.8}$$

In this choice of normalization, both $\hat{R}_w$ and R_f are positive for $Le_D > 1$ and negative for $Le_D < 1$. Note that this choice of R_f and $\hat{R}_w$ does not limit $R_f/\hat{R}_w < 1$. However, to keep $\hat{P}$ an order-one quantity, $R_f/\hat{R}_w$ should be $\lesssim 1.5$ for a typical value of $\gamma = 1.4$.

For a spherical flame, the mass flux is a constant to leading order and is defined by (2.13),

$$m_0 = s_u = \frac{\mathrm{d}r_f}{\mathrm{d}t} - u|_{r_f^+} = \frac{1}{T_{ad}}\frac{\mathrm{d}r_f}{\mathrm{d}t} \tag{3.9}$$

and the leading-order stretch rate is obtained from (2.21),

$$\kappa = \frac{2}{r_f}\frac{\mathrm{d}r_f}{\mathrm{d}t}. \tag{3.10}$$

The results of (3.6) and (3.7) may be substituted into (2.27), (2.30), and (2.31) to determine the evolution of a spherical flame, to be presented next.

3.1. *Off-stoichiometric mixtures*

For the off-stoichiometric mixtures, (2.31) governs the flame propagation rate. For spherical flames in spherical confinement this equation becomes

$$s_u^2 \ln s_u^2 = s_u^2 \left(\frac{R_f}{\hat{R}_w} \right)^3 + \frac{\mathrm{d}s_u}{\mathrm{d}R_f} - \frac{2}{R_f} s_u. \tag{3.11}$$

First, (3.11) will be examined in the unconfined case corresponding to $|\hat{R}_w| \to \infty$. This reduces to equation (5) in Matalon & Bechtold (1987) and equation (42) in Ronney & Sivashinsky (1989) when the diffusivity is a constant. As this equation is an ordinary differential equation, it may be easily solved numerically; however an analytical solution is not possible.

Figure 1 shows the flame speed as a function of radius determined by numerically solving (3.11) with various initial conditions. As seen in figure 1(*a*), any initial condition supplied for $Le_D < 1$ corresponds to a physical solution as $|R_f| \to \infty$. However, figure 1(*b*) shows that only initial conditions along the separatrix solution (bold line) correspond to physically realistic solutions at large radius. The unphysical nature of additional solutions is typical in SVF formulations as has been discussed previously (Matalon & Bechtold 1987; Ronney & Sivashinsky 1989). In the present discussion, the separatrix solution will be interpreted as the physical solution and therefore only the separatrix solution will be shown in the comparisons to follow. In order to generate the separatrix solutions numerically, $Le_D < 1$ flames are given an arbitrary initial condition at a very small radius and the initial-condition-dependent part of the solution is ignored. For $Le_D > 1$ flames, the solutions are obtained by numerically solving backwards in time from the flame at infinite radius having a flame speed of unity. For confined flames, this condition at infinity is arbitrary, but a reverse solution in time becomes stable and allows the determination of the separatrix solution.

Using the physically realistic separatrix solutions, the influence of spherical confinement on flame propagation may now be determined from (3.11). First, it is instructive to look at the temperature perturbation which is causing the change in the flame speed,

$$T_1(0^+) = \left(\frac{R_f}{\hat{R}_w} \right)^3 + \frac{1}{s_u^2} \frac{\mathrm{d}s_u}{\mathrm{d}R_f} - \frac{2}{R_f s_u}. \tag{3.12}$$

The terms on the right-hand side are the result of confinement, flame acceleration, and hydrodynamic stretch respectively. Figure 2 compares the magnitude of these three terms determined by numerically solving (3.11) with $|\hat{R}_w| = 50$. For both $Le_D > 1$ and $Le_D < 1$ flames, the modification to the temperature perturbation as a result of compression is identical and is a positive influence. Therefore adiabatic compression of the unburned gas increases the flame speed, s_u. This term is the dominant influence when the flame is at large radius. The magnitude of the influence is identical at a given $|R_f|$ for both the $Le_D > 1$ and $Le_D < 1$ flames.

Modification of the temperature perturbation from the flame acceleration is seen to be of large magnitude only for flames of small radii. This influence is positive for both the $Le_D > 1$ and $Le_D < 1$ flames. This indicates that the flame acceleration increases the flame speed for both $Le_D > 1$ and $Le_D < 1$ flames at small radii. The magnitude

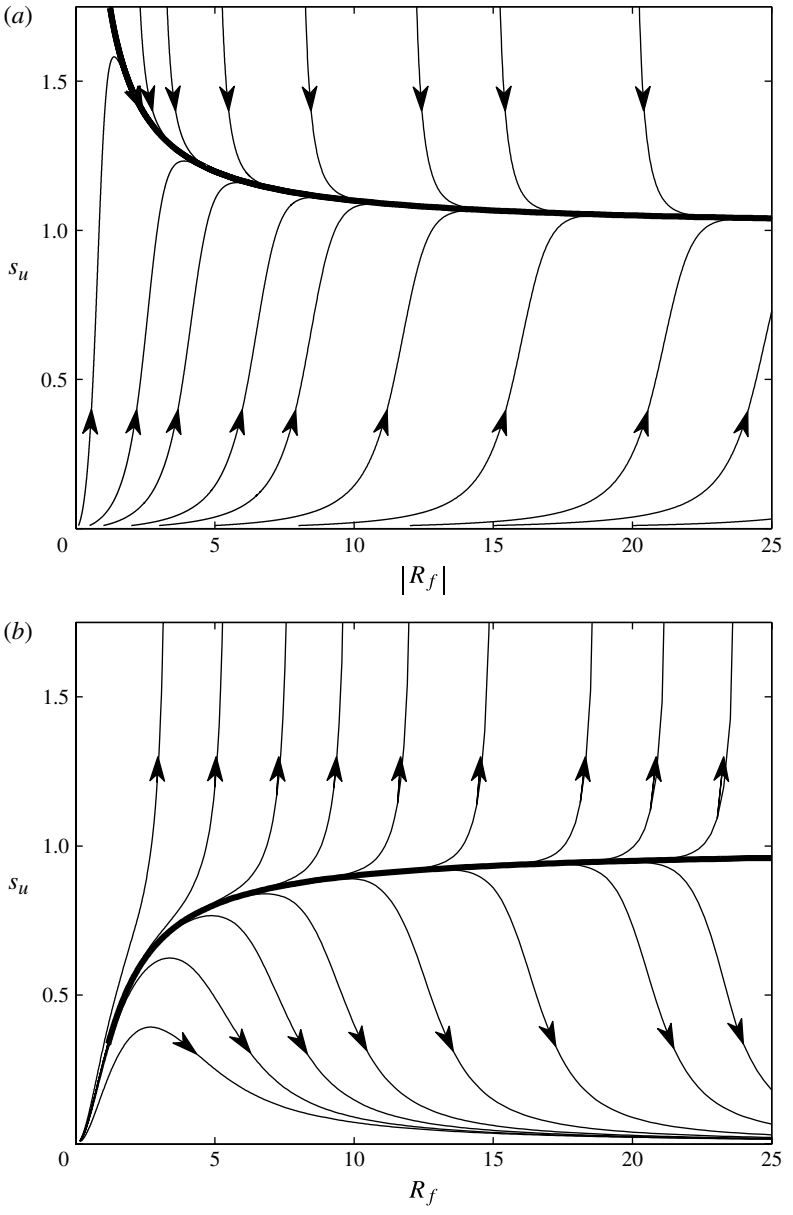

FIGURE 1. Unconfined flame speed as a function of flame radius as determined by (3.11) for (*a*) $Le_D < 1$ and (*b*) $Le_D > 1$. $|\hat{R}_w| \to \infty$. Different curves correspond to different solutions of (3.11) depending on the initial condition supplied. Arrows indicate temporal variation of the flame position. It is seen that all initial conditions for $Le_D < 1$ correspond to physically meaningful solutions as $|R_f| \to \infty$. However, for $Le_D > 1$, only one initial condition results in a physically realistic solution as $|R_f| \to \infty$. The separatrix solution, corresponding to the physically realistic solution to (3.11) is shown as a bold line.

for the $Le_D > 1$ flame is seen to be larger than that for the $Le_D < 1$ flame. For an unconfined flame, the acceleration term would vanish at large radii. However, for the confined case, the confinement causes the flame to increase in speed, which feeds

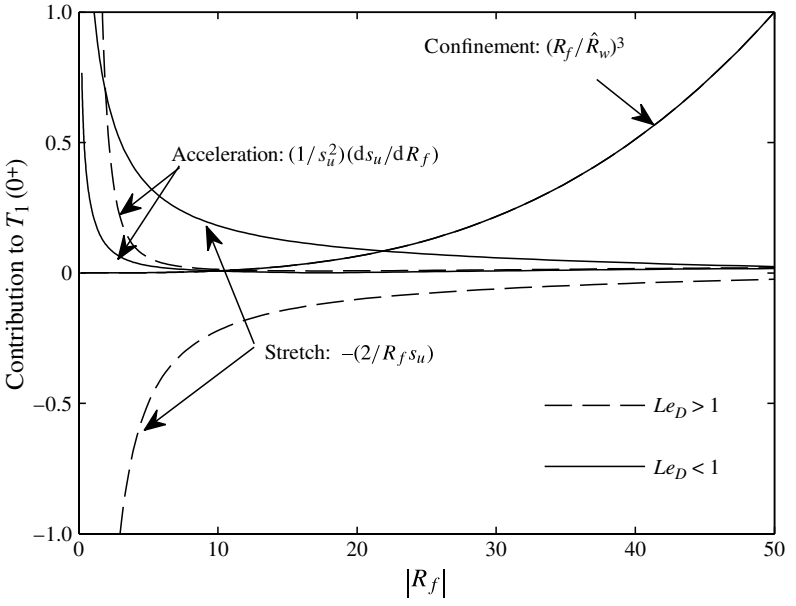

FIGURE 2. Temperature perturbation terms given by (3.12) as a function of flame radius. $|\hat{R}_w| = 50$.

back to the acceleration term. Although the magnitude of the influence is small for the present case, the acceleration at larger radii results in a positive influence for the $Le_D > 1$ case and a negative influence for the $Le_D < 1$ case.

The stretch term is dominant at small radii and its magnitude is always larger than that of the acceleration term. Additionally, for the unconfined case, the acceleration is only significant at very small radii whereas the stretch term remains at slightly larger radii. The influence of stretch is to increase the flame speed and temperature perturbation for the $Le_D < 1$ flame while the opposite influence is observed for the $Le_D > 1$ flame.

The magnitude of the acceleration and stretch terms is uniformly larger at a given $|R_f|$ for $Le_D > 1$ than it is for $Le_D < 1$. However, since the two terms are of opposite sign, the net influence is not as large as that for the $Le_D < 1$ flame at small radii.

Figure 3 plots the flame speed as a function of (*a*) R_f and (*b*) stretch rate as determined by (3.11) for various radii of the confining vessel, $|\hat{R}_w|$. As was expected from the analysis of the temperature perturbation term, the $Le_D > 1$ flame is seen to have a flame speed less than unity for small radii. This is a result of the negative influence of stretch on the flame speed for $Le_D > 1$ flames. For $Le_D < 1$ flames, the flame speed is initially greater than unity at small radii as a result of both stretch and acceleration.

At large radii, the flame speeds of both $Le_D > 1$ and $Le_D < 1$ flames are seen to increase. This is a result of the confinement term dominating at larger radii. As the chamber radius $\hat{R}_w$ is decreased, it is seen that the influence of confinement is manifested at smaller flame radii. For both $Le_D > 1$ and $Le_D < 1$ flames, the behaviour at large radii is nearly identical. This is a result of the dominance of the confinement term which influences both Lewis number flames similarly.

Experimental investigations are particularly concerned with the influence of pressure on spherical flame propagation as spherical flames are often used for the determination

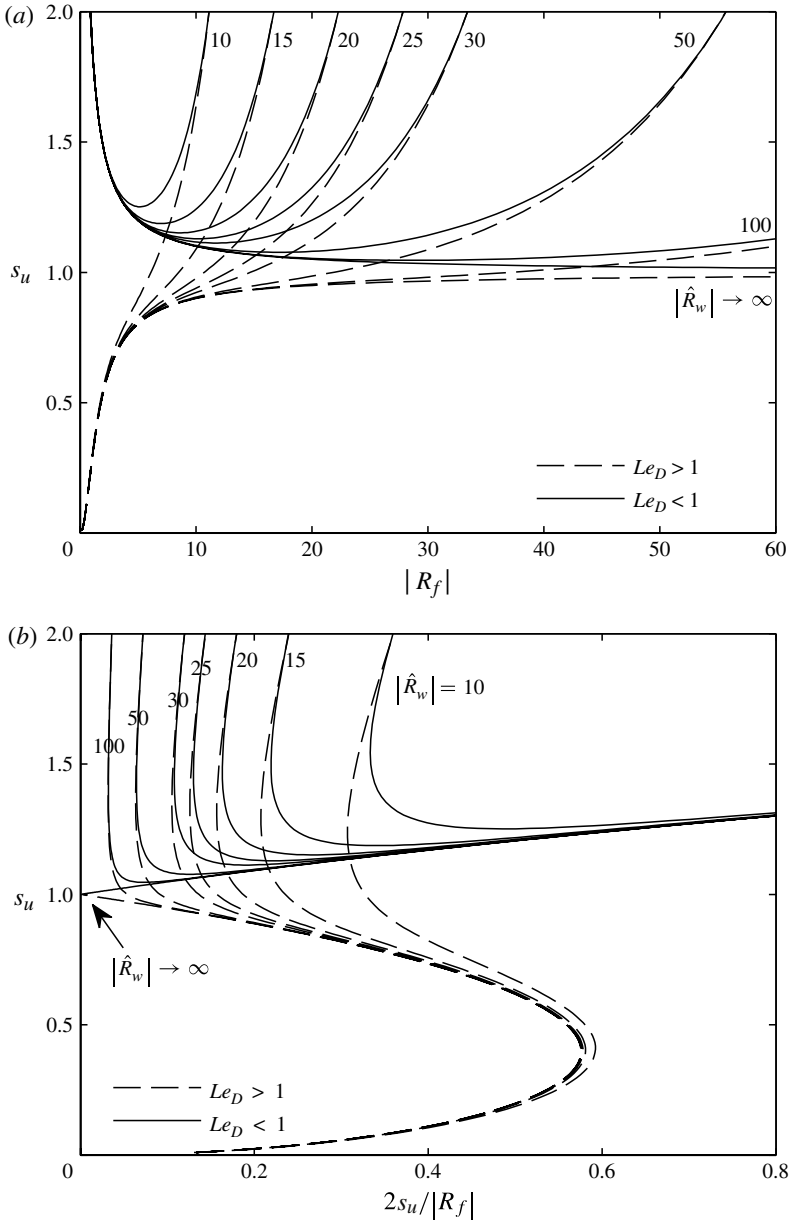

FIGURE 3. Separatrix solutions of (3.11) for various confining vessel radii, $|\hat{R}_w|$. Flame speed as a function of (*a*) flame radius, (*b*) stretch rate.

of laminar flame speeds. In these measurements, experimental data from early flame propagation are used as they are assumed to be uninfluenced by the increase in pressure resulting from the confining volume. The present analysis allows an exact determination of the radius at which this approximation is no longer valid.

In order to assess the flame radius at which the confining volume influences the flame propagation rate, figure 4 plots the flame radius at which a given percentage change in flame speed is predicted by (3.11) as a function of chamber wall

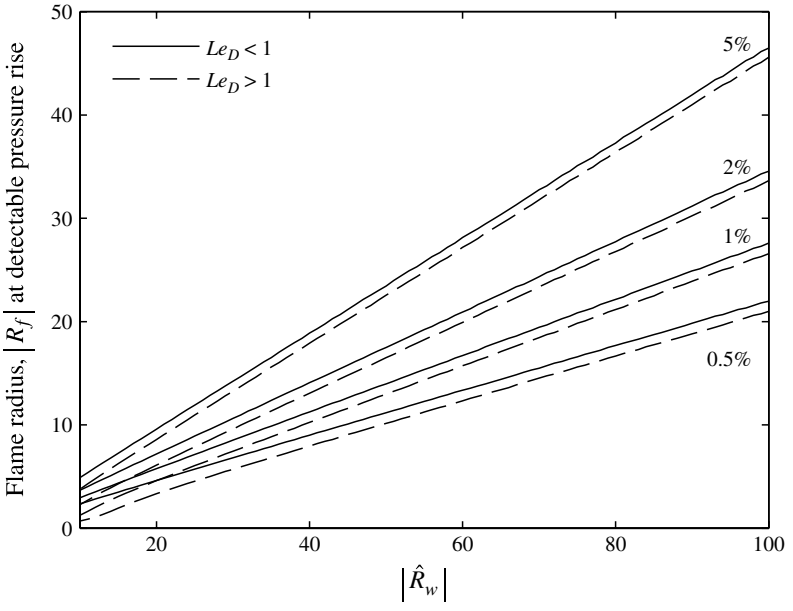

FIGURE 4. Flame radius at which the flame speed is noticeably influenced by confinement as a function of confinement radius. The percentage change in the flame speed due to confinement is indicated on the graph.

radius, $|\hat{R}_w|$. It is seen that the radius at which the flame speed is influenced by the confinement is linearly proportional to the chamber wall radius. Additionally, $Le_D < 1$ flames are seen to be affected by the confining volume at a slightly larger radius than that of the $Le_D > 1$ flames.

3.2. *Near-stoichiometric mixtures*

The criterion to determine whether the excess or the deficient reactant is locally in excess comes from (2.22). For the spherical flame, the equation becomes

$$Y_{E,1}(0^+) - Y_{D,1}(0^+) = \varphi + \frac{1}{qs_u^2}\left(\frac{\mathrm{d}s_u}{\mathrm{d}R_f} - \frac{2}{R_f}s_u\right)\left(\frac{I_E}{I_D} - 1\right). \tag{3.13}$$

It is of interest to note the state when the right-hand side of (3.13) switches sign, as this determines which reactant is locally deficient. As φ is always a positive quantity, the sign can only switch when the sum of the flame acceleration and hydrodynamic stretch multiplied by the preferential diffusion term, $(I_E/I_D - 1)$, is negative. This switching can be predicted by first assuming that the near-stoichiometric flames will behave qualitatively similarly to off-stoichiometric flames. Looking at figure 2, it is seen that the hydrodynamic stretch term always dominates over the acceleration term. Therefore, the sum of the hydrodynamic stretch and acceleration terms is positive for $Le_D < 1$ and negative for $Le_D > 1$. The preferential diffusion term is positive when $Le_E > Le_D > 1$ or $Le_E < Le_D < 1$. From these results, switching may be predicted to occur only for the case where $Le_E > Le_D$.

When the right-hand side of (3.13) is greater than zero, reactant $\mathscr{M}_E$ is locally in excess and the appropriate evolution equation is (2.27). For spherical flames, this

becomes

$$s_u^2 \ln s_u^2 - s_u^2 \ln \left[\frac{\mathscr{G}\left(a, b; \dfrac{qY_{E,1}(0^+)}{Le_E}\right)}{\mathscr{G}\left(a, b; \dfrac{q\varphi}{Le_E}\right)} \right] = s_u^2 \left(\frac{R_f}{\hat{R}_w}\right)^3 + \frac{\mathrm{d}s_u}{\mathrm{d}R_f} - \frac{2}{R_f} s_u, \tag{3.14}$$

where

$$Y_{E,1}(0^+) = \varphi + \frac{1}{q s_u^2} \left(\frac{\mathrm{d}s_u}{\mathrm{d}R_f} - \frac{2}{R_f} s_u \right) \left(\frac{I_E}{I_D} - 1 \right). \tag{3.15}$$

When the right-hand side of (3.13) is less than zero, reactant $\mathscr{M}_D$ is locally in excess and the appropriate evolution equation is (2.30). For spherical flames, this becomes

$$s_u^2 \ln s_u^2 - s_u^2 \ln \left[\frac{\mathscr{G}\left(b, a; \dfrac{qY_{D,1}(0^+)}{Le_D}\right)}{\mathscr{G}\left(a, b; \dfrac{q\varphi}{Le_E}\right)} \right] = s_u^2 \left(\frac{R_f}{\hat{R}_w}\right)^3 + s_u^2 \varphi q + \left(\frac{\mathrm{d}s_u}{\mathrm{d}R_f} - \frac{2}{R_f} s_u \right), \frac{I_E}{I_D} \tag{3.16}$$

where

$$Y_{D,1}(0^+) = -\varphi - \frac{1}{q s_u^2} \left(\frac{\mathrm{d}s_u}{\mathrm{d}R_f} - \frac{2}{R_f} s_u \right) \left(\frac{I_E}{I_D} - 1 \right). \tag{3.17}$$

For mixtures near stoichiometric, the governing equations are (3.14) and (3.16). The separatrix solutions to these equations may be plotted while monitoring (3.13) to determine which reactant is completely consumed. The results are qualitatively similar to the findings of Bechtold & Matalon (1999) for counterflow flames.

Figures 5 and 6 show the flame speed as a function of stretch for unconfined, near-stoichiometric mixtures with various Lewis numbers. In figure 5(*a*) it is seen that, for $Le_D > 1$ mixtures, the flame behaves differently for near-stoichiometric mixtures than it does for off-stoichiometric mixtures. In the case of unconfined off-stoichiometric mixtures, the flame speed is less than unity. For near-stoichiometric mixtures with small values of Le_E, it is seen that the flame speed is no longer monotonic and can indeed be greater than unity. In this case, $Y_{E,1}(0^+) > \varphi$. This occurs due to the higher mass diffusion rate of species $\mathscr{M}_E$ relative to that of $\mathscr{M}_D$ resulting in an increased concentration of $\mathscr{M}_E$ at the flame. This increase in the concentration of $\mathscr{M}_E$ causes an increase in the reaction rate and thus the flame speed which results in a flame speed greater than unity at low stretch rates. However, the flame temperature perturbation $T_1(0^+)$ is typically negative for $Le_D > 1$. Therefore, at higher stretch rates, the flame speed is less than unity.

Figure 5(*b*) demonstrates that the deficient reactant can be locally in excess when $Le_E > Le_D$. As $\mathscr{M}_D$ is the more mobile reactant in this case, its concentration can exceed that required for stoichiometric combustion and therefore the initially excess reactant $\mathscr{M}_E$ is completely consumed and is locally deficient.

Figure 6 shows the flame speed as a function of stretch for the $Le_D < 1$ case. Again, the excess reactant can be locally deficient when $Le_E > Le_D$. For the case where $Le_E > 1 > Le_D$, it is seen that the flame qualitatively changes at the location where the excess reactant becomes locally deficient. This results from the

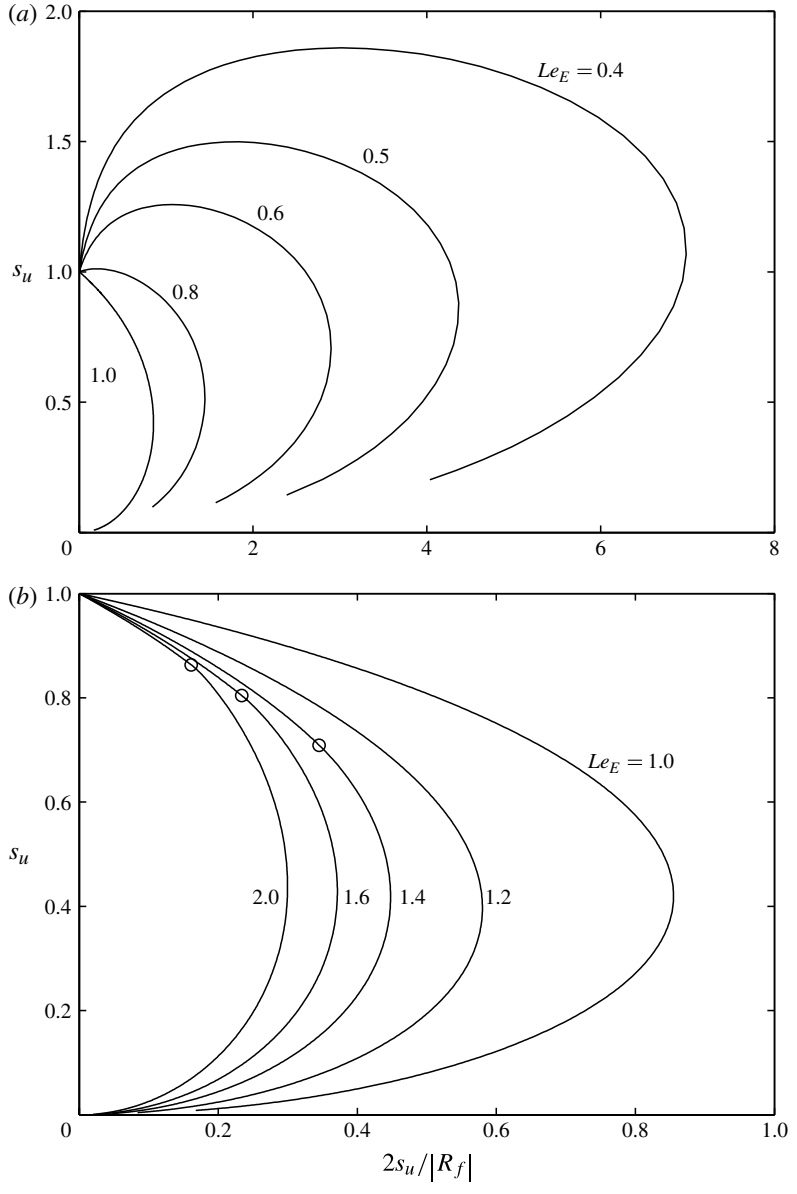

FIGURE 5. Separatrix solutions of (3.14) and (3.16) for various values of Le_E with (*a*) $Le_E \leqslant 1$; (*b*) $Le_E \geqslant 1$. $Le_D = 1.2$, $\lambda = T$, $T_{ad} = 5$, $a = b = 1$, $\varphi = 0.1$. Circles denote the switching between the excess and deficient reactants being locally deficient.

excess reactant's Lewis number dominating when the excess is locally deficient. Consequently the flame speed tends to be lower than unity, although the increased concentration of $\mathscr{M}_D$ has a positive influence on the flame speed at low stretch rates.

For near-stoichiometric mixtures, the flame initially propagates similarly to the unconfined case just presented. However, at large radii, the influence of confinement

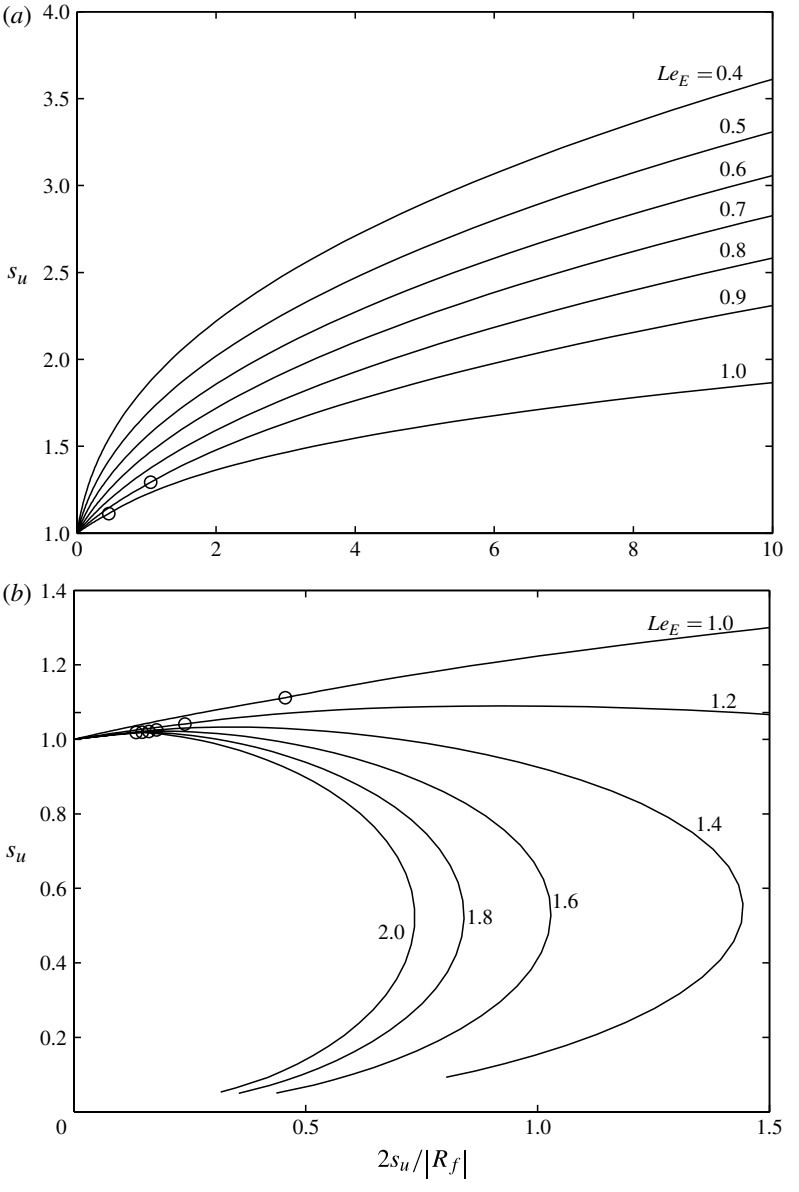

FIGURE 6. Separatrix solutions of (3.14) and (3.16) for various values of Le_E with (*a*) $Le_E \leqslant 1$; (*b*) $Le_E \geqslant 1$. $Le_D = 0.8$, $\lambda = T$, $T_{ad} = 5$, $a = b = 1$, $\varphi = 0.1$. Circles denote the switching between the excess and deficient reactants being locally deficient.

causes an increase in the flame speed, as was seen in the confined, off-stoichiometric case. In the interest of space, the results of these calculations are not shown.

4. Extrapolation of laminar flame speeds

The extrapolation of the laminar flame speed has historically assumed a linear relationship between stretch and flame speed as was determined asymptotically by

Matalon & Matkowsky (1982) and applied to experiments by Wu & Law (1984). For the outwardly propagating flame, the linear relationship between stretch and flame speed takes the form

$$s_u\left(1+\frac{1}{R_f}\right)=1. \tag{4.1}$$

This equation has been used by numerous authors (e.g. Dowdy *et al.* 1990; Bradley *et al.* 1998; Jerzembeck *et al.* 2009) to extrapolate experimental measurements and determine the unstretched laminar flame speed. Equation (4.1) was derived from the assumption that the Lewis number of the mixture is near unity and that the flame speed is the unstretched value to leading order. The present derivation removes these restrictions and is therefore a more general result which may be applied either to mixtures with large Lewis numbers or to flames that are highly stretched. For an off-stoichiometric, unconfined mixture, the present analysis suggests the following relationship between the flame speed and the flame radius:

$$s_u^2\ln s_u^2=\frac{\mathrm{d}s_u}{\mathrm{d}R_f}-\frac{2}{R_f}s_u. \tag{4.2}$$

This equation has been derived previously by Matalon & Bechtold (1987) and later by Ronney & Sivashinsky (1989). Ideally, this equation could be used for extrapolating experimental measurements to determine the unstretched laminar flame speed. However, it is numerically unstable, as demonstrated earlier, and presents difficulty in experimental implementation due to the derivative term. Therefore, it was suggested (Kelley & Law 2009) that a nonlinear relationship between stretch and flame speed should be used for the extrapolation of the laminar flame speed from experimental data. The extrapolation proposed was based on a quasi-steady version of (4.2),

$$s_u^2\ln s_u^2=-\frac{2}{R_f}s_u. \tag{4.3}$$

The use of the quasi-steady approximation is prevalent in several derivations (e.g. Frankel & Sivashinsky 1984; Chen & Ju 2007) and (4.3) has subsequently been used by many authors (e.g. Halter, Tahtouh & Mounaïm-Rousselle 2010; Singh, Nishiie & Qiao 2011) for the extrapolation of laminar flame speeds. However, as seen in figure 2, the acceleration term is only negligible when the flame is reasonably large and this was noted in Kelley & Law (2009).

A recent publication by Chen (2011) confirmed that (4.3) improves upon the use of (4.1) in the extrapolation of laminar flame speeds. This was demonstrated by numerically simulating methane flames and using various extrapolation equations to determine the unstretched flame speed. Chen noted, however, that the use of an alternative extrapolation equation,

$$s_u=1-\frac{1}{R_f}, \tag{4.4}$$

appeared to give even better results than (4.3) for $Le_D>1$. However, (4.4) was found to be less accurate than (4.3) for $Le_D<1$. The difference in the extrapolated flame speeds for (4.3) and (4.4) was very small and both were shown to be significant improvements over (4.1).

It is noted that (4.4) was first proposed by Markstein (1951) and was originally an empirical assumption. Chen (2011) noted that (4.1), (4.3) and (4.4) are all identical when expanded in powers of R_f^{-1} to first order, although no mathematical explanation was given for the apparent improved accuracy of (4.4) over (4.3). It is now demonstrated that the present analysis gives a rigorous mathematical explanation for the findings of Chen. Expanding (4.2), (4.3), and (4.4) in inverse powers of R_f, the following relationships are obtained.

Expansion of (4.2), the present asymptotic result:

$$s_u\left[1+\frac{1}{R_f}+\frac{1}{R_f^2}+\frac{2}{3}\frac{1}{R_f^3}+O\left(\frac{1}{R_f^4}\right)\right]=1. \tag{4.5}$$

Expansion of (4.3), the quasi-steady approximation:

$$s_u\left[1+\frac{1}{R_f}+\frac{3}{2}\frac{1}{R_f^2}+\frac{8}{3}\frac{1}{R_f^3}+O\left(\frac{1}{R_f^4}\right)\right]=1. \tag{4.6}$$

Expansion of (4.4), Markstein's empirical equation:

$$s_u\left[1+\frac{1}{R_f}+\frac{1}{R_f^2}+\frac{1}{R_f^3}+O\left(\frac{1}{R_f^4}\right)\right]=1. \tag{4.7}$$

Comparing (4.5), (4.6) and (4.7), the mathematical explanation for the findings of Chen become clear. To first order in inverse powers of R_f, all of these equations are identical to the linear extrapolation, (4.1), which has been used historically. The equations, however, differ at second order. Markstein's empirical equation, (4.4), is identical to the present asymptotic equation, (4.2), up to second order while the quasi-steady approximation, (4.3), differs at second order.

Chen (2011) found that Markstein's equation provided a slight improvement over the use of (4.3) for $Le_D > 1$ mixtures. It is expected, based on the above analysis, that this equation would be found to be an improvement for all mixtures, not just $Le_D > 1$. The fact that Chen found an improvement when using Markstein's equation implies that the acceleration term present in (4.2) is important at small radii, as was discussed in § 3.1. It also suggests that the use of the quasi-steady approximation in any derivation restricts the qualitative and quantitative analysis to flames of large radii.

At the third order in inverse powers of R_f, Markstein's equation begins to differ from the present asymptotic result. It is therefore proposed that a third-order expansion such as that of (4.5) would provide improved accuracy over Markstein's in the extrapolation of laminar flame speeds from experimental measurements as this more closely approximates (4.2). Figure 7 compares the present asymptotic equation, (4.2), the quasi-steady approximation, equation (4.3), the presently proposed extrapolation equation, (4.5), Markstein's equation, (4.4), and the historical linear extrapolation, (4.1). It is seen that the present asymptotic result, shown as the bold line, is closely approximated by (4.5) for all Le_D. Interestingly, (4.5) closely approximates (4.2) for small R_f when $Le_D > 1$. Markstein's equation (4.4) closely approximates (4.2) for $Le_D < 1$ but is seen to deviate for $Le_D > 1$. Equation (4.3) is seen to deviate even further from (4.2).

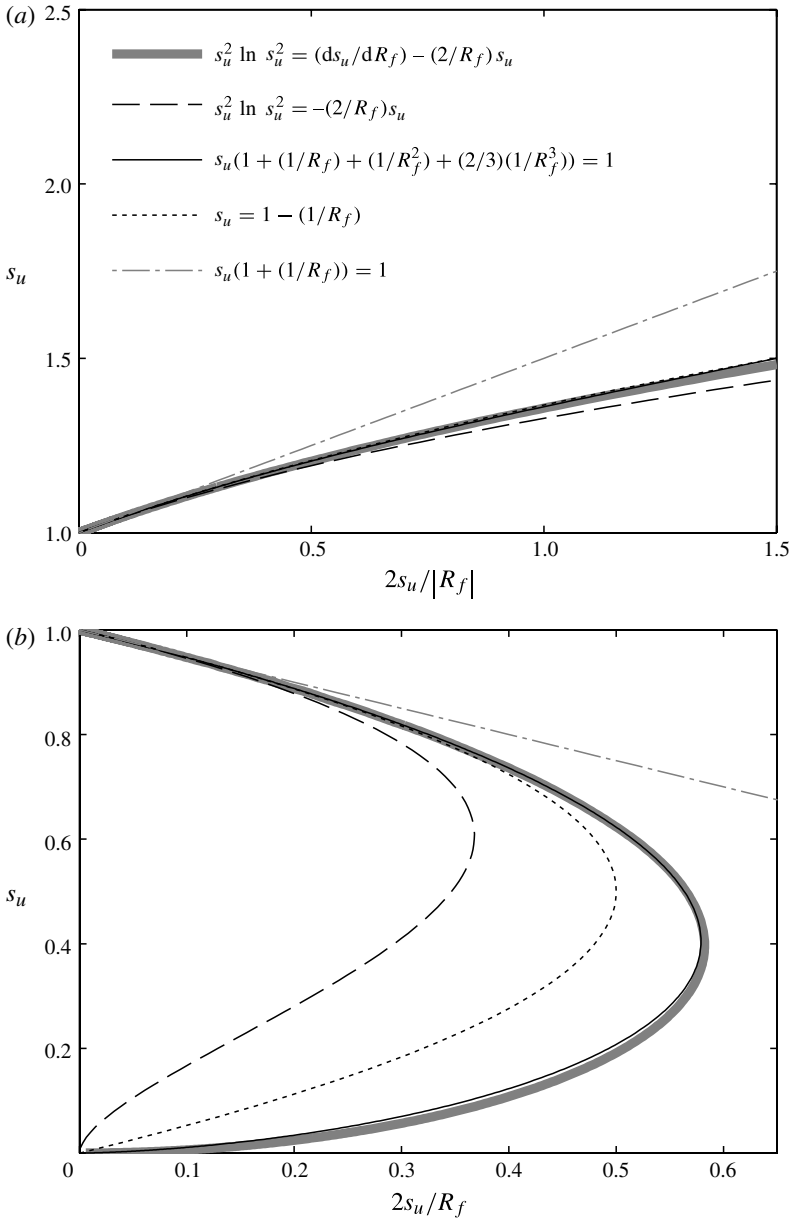

FIGURE 7. Comparison of extrapolation equations in the literature: the present asymptotic equation, (4.2), the quasi-steady approximation, (4.3), the presently proposed extrapolation equation, (4.5), Markstein's equation, (4.4) and the linear equation, (4.1): (*a*) $Le_D < 1$; (*b*) $Le_D > 1$.

Figure 7 therefore clearly demonstrates the merit of using (4.5) in extrapolations as it is a very close approximation to (4.2) and is therefore the most accurate of the extrapolation equations proposed. In order to use (4.5) in the experimental extrapolation of laminar flame speeds, it is useful to integrate the equation to yield the relationship between the flame radius and time, which are the two experimentally

measured quantities,

$$\tilde{s}_b^0\tilde{t} + \tilde{c} = \tilde{r}_f + 2\tilde{L}_b \ln \tilde{r}_f - 4\frac{\tilde{L}_b^2}{\tilde{r}_f} - \frac{8}{3}\frac{\tilde{L}_b^3}{\tilde{r}_f^2}. \tag{4.8}$$

Here, the extrapolation equation is expressed in dimensional form, as this is the most useful form for experimental data analysis. A downstream Markstein length has been defined as $\tilde{L}_b = \tilde{\ell}\tilde{E}_a I_D/2\tilde{T}_{ad}\tilde{R}^0$. The variable $\tilde{c}$ is an integration constant. The parameters, $\tilde{c}$, $\tilde{L}_b$, and $\tilde{s}_b^0$ may be obtained by fitting (4.8) to experimental measurements of the radius of a flame as a function of time, thus yielding a measurement of the downstream Markstein length and the unstretched laminar flame speed.

It is important to note that the use of (4.8) will provide only a slight improvement over the integrated form of (4.3) found in Kelley & Law (2009). However, (4.8) is much easier to use in a numerical regression. To compare the differences in experimental extrapolations, the experimental data presented in Kelley *et al.* (2011) have been re-analysed. In that publication, the extrapolation of atmospheric pressure data were shown to have the strongest influence from stretch and therefore the highest sensitivity to the extrapolation equation employed. Therefore, the atmospheric pressure measurements for *n*-pentane will be used as an example case. The integrated forms of (4.1), (4.3), (4.4) and (4.5) are used to extrapolate the experimental measurements of the radius of the flame as a function of time to determine the unstretched laminar flame speed and the Markstein length. The results of these extrapolations are shown in figure 8. The use of the integration of (4.1) clearly results in a higher extrapolation of the laminar flame speed than the other extrapolation equations for lean and rich mixtures although the difference is negligible around $\phi = 1.3$. The other three extrapolation equations are nearly identical in the extrapolation of laminar flame speeds seen in figure 8(*a*). Therefore, the use of the extrapolation procedure presented in Kelley & Law (2009) or the proposed improvement of (4.8) provide nearly identical flame speed measurements which are well within typical experimental uncertainty. However, the experimental measurement of the Markstein length, shown in figure 8(*b*), does depend more sensitively on the extrapolation equation employed. Specifically, while the present extrapolation equation (4.8) is seen to yield similar results to an extrapolation using Markstein's equation, the use of the quasi-steady extrapolation proposed in Kelley & Law (2009) results in larger magnitude Markstein lengths for rich mixtures.

5. Concluding remarks

Using large-activation-energy asymptotics, confined premixed flames were analysed and their evolution was determined. The present derivation describes the evolution of a premixed flame with general Lewis number, general equivalence ratio, temperature-dependent transport coefficients, general reaction orders, and weak pressure rise. Under the assumption of weak pressure rise, the primary influence of confinement was to adiabatically compress the unburned gas which resulted in a positive perturbation to the downstream flame temperature and an order-one response of the flame propagation speed.

The specific case of a spherical flame propagating in a spherical chamber was analysed to determine the influence of confinement. Mixtures with widely varying Lewis numbers were found to have a similar response to confinement on a normalized flame radius length scale, R_f. The radius at which confinement begins to influence

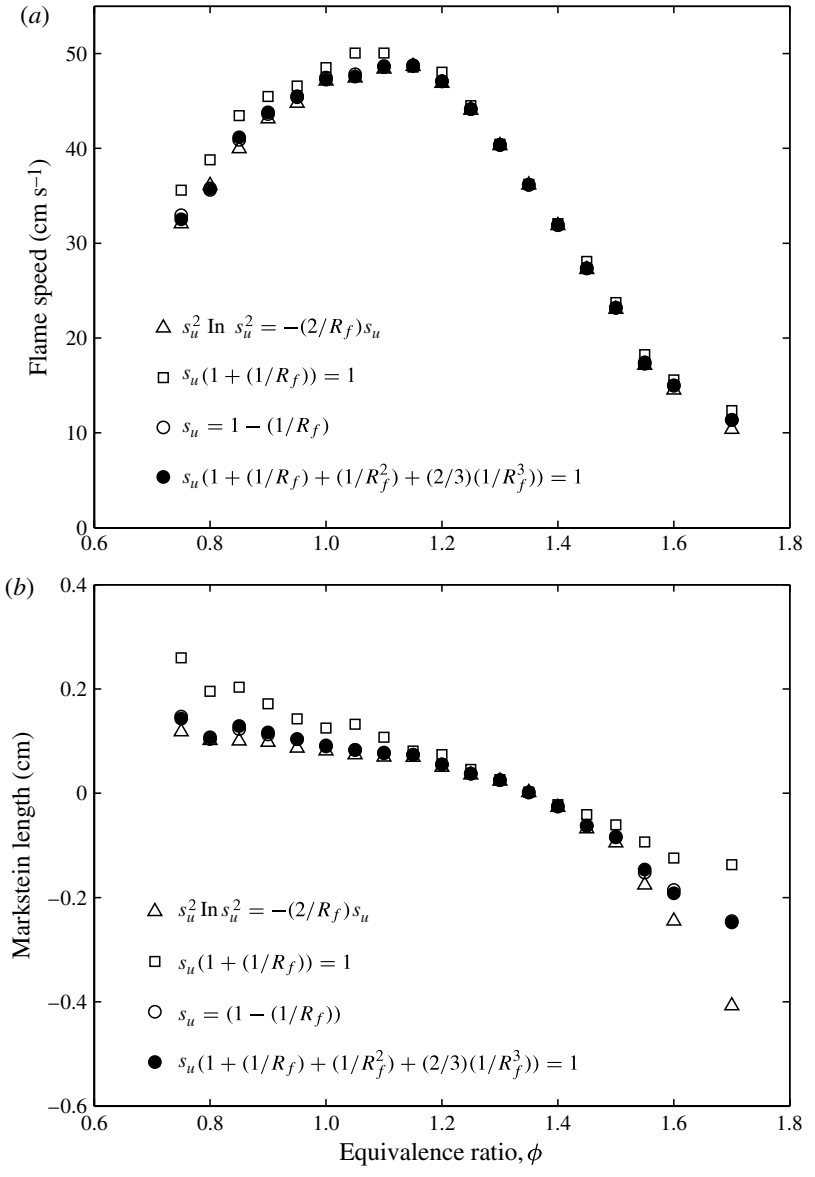

FIGURE 8. (*a*) Laminar flame speeds and (*b*) Markstein lengths extrapolated using various extrapolation equations from experimental data for atmospheric pressure *n*-pentane/air outwardly propagating flames originally published in Kelley *et al.* (2011).

flame propagation was determined and was found to be linearly proportional to the radius of the confining vessel.

For near-stoichiometric mixtures, the initially deficient reactant was found to be locally in excess when the flame was at small radii for mixtures with $Le_E > Le_D$. This was attributed to the high mobility of the deficient reactant. Near-stoichiometric mixtures with $Le_D > 1 > Le_E$ were found to have flame speeds which could exceed the unstretched laminar flame speed at certain flame radii. This was attributed to the

increased concentration of the excess reactant at the flame front which results in an increased reaction rate.

The extrapolation of the laminar flame speed from experimental measurements of the flame radius as a function of time is dependent on the equation used for extrapolation. An improved extrapolation equation, (4.8), was presented. It was found to provide nearly identical extrapolations of the laminar flame speed as the extrapolation equation presented in Kelley & Law (2009); however the extrapolated Markstein lengths were found to differ.

Acknowledgements

This research was supported by the Air Force Office of Scientific Research under the technical monitoring of Dr Julian M. Tishkoff and by the National Science Foundation under grant number DMS-0807340.

REFERENCES

BECHTOLD, J. K. & MATALON, M. 1999 Effects of stoichiometry on stretched premixed flames. *Combust. Flame* **119**, 217–232.

BECHTOLD, J. K. & MATALON, M. 2000 Some new results on Markstein number predictions. *38th Aerospace Sciences Meeting & Exhibit, AIAA Paper* 2000-0575.

BOUVET, N., CHAUVEAU, C., GÖKLAP, I. & HALTER, F. 2011 Experimental studies of the fundamental flame speeds of syngas (H_2/CO)/air mixtures. *Proc. Combust. Inst.* **33**, 913–920.

BRADLEY, D., HICKS, R. A., LAWES, M., SHEPPARD, C. G. W. & WOOLLEY, R. 1998 The measurement of laminar burning velocities and Markstein numbers for iso-octane-air and iso-octane-n-heptane-air mixtures at elevated temperatures and pressure in an explosion bomb. *Combust. Flame* **115**, 126–144.

BRADLEY, D. & MITCHESON, A. 1976 Mathematical solution for explosions in spherical vessels. *Combust. Flame* **26**, 201–217.

BUCKMASTER, J. & LEE, C. J. 1992 The effects of confinement and heat loss on outwardly propagating spherical flames. *Twenty-Fourth Symposium (Intl) on Combustion*, pp. 45–51. The Combustion Institute.

BUCKMASTER, J. D. 1977 Slowly varying laminar flames. *Combust. Flame* **28**, 225–239.

BUCKMASTER, J. D. & LUDFORD, G. S. S. 1982 *Theory of Laminar Flames*. Cambridge University Press.

BUSH, W. B. & FENDELL, F. E. 1970 Asymptotic analysis of laminar flame propagation for general Lewis numbers. *Combust. Sci. Technol.* **1**, 421–428.

CHEN, Z. 2011 On the extraction of laminar flame speed and Markstein length from outwardly propagating spherical flames. *Combust. Flame* **158**, 291–300.

CHEN, Z., BURKE, M. P. & JU, Y. 2009 Effects of compression and stretch on the determination of laminar flame speeds using propagating spherical flames. *Combust. Theor. Model.* **13**, 343–364.

CHEN, Z. & JU, Y. 2007 Theoretical analysis of the evolution from ignition kernel to flame ball and planar flame. *Combust. Theor. Model.* **11**, 427–435.

CLAVIN, P., PELCÉ, P. & HE, L. 1990 One-dimensional vibratory instability of planar flames propagating in tubes. *J. Fluid Mech.* **216**, 299–322.

DOWDY, D. R., SMITH, D. B., TAYLOR, S. C. & WILLIAMS, A. 1990 The use of expanding spherical flames to determine burning velocities and stretch effects in hydrogen/air mixtures. *Twenty-Third Symposium (Intl) on Combustion*, pp. 325–332. The Combustion Institute.

ESCHENBACK, R. C. & AGNEW, J. T. 1958 Use of the constant-volume bomb technique for measuring burning velocity. *Combust. Flame* **2**, 273–285.

FRANKEL, M. L. & SIVASHINSKY, G. I. 1984 On quenching of curved flames. *Combust. Sci. Technol.* **40**, 257–268.

HALTER, F., TAHTOUH, T. & MOUNAÏM-ROUSSELLE, C. 2010 Nonlinear effects of stretch on the flame front propagation. *Combust. Flame* **157**, 1825–1832.

JERZEMBECK, S., PETERS, N., PEPIOT-DESJARDINS, P. & PITSCH, H. 2009 Laminar burning velocities at high pressure for primary reference fuels and gasoline: experimental and numerical investigation. *Combust. Flame* **156**, 292–301.

JOMAAS, G., LAW, C. K. & BECHTOLD, J. K. 2007 On transition to cellularity in expanding spherical flames. *J. Fluid Mech.* **583**, 1–26.

KELLER, D. & PETERS, N. 1994 Transient pressure effects in the evolution equation for premixed flame fronts. *Theor. Comput. Fluid Dyn.* **6**, 141–159.

KELLEY, A. P. & LAW, C. K. 2009 Nonlinear effects in the extraction of laminar flame speeds from expanding spherical flames. *Combust. Flame* **156**, 1844–1851.

KELLEY, A. P., SMALLBONE, A. J., ZHU, D. L. & LAW, C. K. 2011 Laminar flame speeds of C_5 to C_8 n-alkanes at elevated pressures: experimental determination, fuel similarity, and stretch sensitivity. *Proc. Combust. Inst.* **33**, 963–970.

LEWIS, B. & VON ELBE, G. 1961 *Combustion, Flames, and Explosions of Gases*, 2nd edn. Academic.

MARKSTEIN, G. H. 1951 Experimental and theoretical studies of flame-front stability. *J. Aeronaut. Sci.* **18**, 199–209.

MATALON, M. & BECHTOLD, J. K. 1987 Spherically expanding flames. *Proc. 1987 ASME/JSME Thermal Engineering Joint Conference*, vol. 1, pp. 95–101.

MATALON, M., CUI, C. & BECHTOLD, J. K. 2003 Hydrodynamic theory of premixed flames: effects of stoichiometry, variable transport coefficients and arbitrary reaction orders. *J. Fluid Mech.* **487**, 179–210.

MATALON, M. & MATKOWSKY, B. J. 1982 Flames as gasdynamic discontinuities. *J. Fluid Mech.* **124**, 239–259.

PELCE, P. & CLAVIN, P. 1982 Influence of hydrodynamics and diffusion upon the stability limits of laminar premixed flames. *J. Fluid Mech.* **124**, 219–237.

PETERS, N. & LUDFORD, G. S. S. 1983 The effect of pressure variations on premixed flames. *Combust. Sci. Technol.* **34**, 331–344.

RAEZER, S. D. 1961 The relationship between burning velocity and space velocity of a spherical combustion wave in a closed spherical chamber. *Combust. Flame* **5**, 77–80.

RONNEY, P. D. & SIVASHINSKY, G. I. 1989 A theoretical study of propagation and extinction of nonsteady spherical flame fronts. *SIAM J. Appl. Maths* **49** (4), 1029–1046.

SINGH, D., NISHIIE, T. & QIAO, L. 2011 Experimental and kinetic modeling study of the combustion of n-decane, Jet-A, and S-8 in laminar premixed flames. *Combusti. Sci. Technol.* **183** (10).

SIVASHINSKY, G. I. 1976 On a distorted flame front as a hydrodynamic discontinuity. *Acta Astronaut.* **3**, 889–918.

SIVASHINSKY, G. I. 1979 Hydrodynamic theory of flame propagation in an enclosed volume. *Acta Astronaut.* **6**, 631–645.

TOGBÉ, C., HALTER, F., FOUCHER, F., MOUNAIM-ROUSESELLE, C. & DAGAUT, P. 2011 Experimental and detailed kinetic modelling study of 1-pentanol oxidation in a JSR and combustion in a bomb. *Proc. Combust. Inst.* **33**, 367–374.

WILLIAMS, F. A. 1994 *Combustion Theory*, 2nd edn. Westview.

WU, C. K. & LAW, C. K. 1984 On the determination of laminar flame speeds from stretched flames. *Twentieth Symposium (Intl) on Combustion*, pp. 1941–1949. The Combustion Institute.

WU, X., WANG, M., MOIN, P. & PETERS, N. 2003 Combustion instability due to the nonlinear interaction between sound and flame. *J. Fluid Mech.* **497**, 23–53.